

## **Structural redetermination, thermal expansion and refractive indices of $\text{KLu}(\text{WO}_4)_2$**

**M. C. Pujol, X. Mateos, A. Aznar, X. Solans, S. Suriñach, J. Massons, F. Díaz and M. Aguiló**

Copyright © International Union of Crystallography

Author(s) of this paper may load this reprint on their own web site provided that this cover page is retained. Republication of this article or its storage in electronic databases or the like is not permitted without prior permission in writing from the IUCr.

Structural redetermination, thermal expansion and refractive indices of  $\text{KLu}(\text{WO}_4)_2$ M. C. Pujol,<sup>a</sup> X. Mateos,<sup>a</sup> A. Aznar,<sup>a</sup> X. Solans,<sup>b</sup> S. Suriñach,<sup>c</sup> J. Massons,<sup>a</sup> F. Díaz<sup>a</sup> and M. Aguiló<sup>a\*</sup><sup>a</sup>Física i Cristal·lografia de Materials (FICMA), Universitat Rovira i Virgili, Campus Sescelades c/ Marcel·lí Domingo, s/n, 43007-Tarragona, Spain, <sup>b</sup>Departament de Cristal·lografia, Mineralogia i Diposits Minerals, Universitat de Barcelona, 08028-Barcelona, Spain, and <sup>c</sup>Departament de Física, Universitat Autònoma de Barcelona, 08193-Bellaterra, Spain. Correspondence e-mail: magdalena.aguiló@urv.net

The crystal structure of monoclinic  $\text{KLu}(\text{WO}_4)_2$  (KLuW) crystals was determined at room temperature by using single-crystal X-ray diffraction data. The unit-cell parameters were  $a = 10.576$  (7),  $b = 10.214$  (7),  $c = 7.487$  (2) Å,  $\beta = 130.68$  (4)°, with  $Z = 4$ , in space group  $C2/c$ . The unit-cell parameters of  $\text{KLu}_{1-x}\text{Yb}_x(\text{WO}_4)_2$  were determined in relation to Yb concentration. Vickers micro-indentations were used to study the microhardness of KLuW. The linear thermal expansion tensor was determined and the principal axis with maximum thermal expansion ( $\alpha'_{33} = 16.72 \times 10^{-6} \text{ K}^{-1}$ ),  $X'_3$ , was located 13.51° from the  $c$  axis. The room-temperature optical tensor was studied in the near-infrared (NIR) and visible range. The principal optical axis with maximum refractive index ( $n_g = 2.113$ ),  $N_g$ , was located 18.5° from the  $c$  axis at 632.8 nm. Undoped and ytterbium-doped KLuW crystals were grown by the TSSG (top-seeded-solution growth) slow-cooling method. The crystals show {110},  $\{111\}$ , {010} and {310} faces that basically constitute the habit of the KLuW crystals.

## 1. Introduction

The monoclinic phases of potassium and rare earth double tungstates  $\text{KRE}(\text{WO}_4)_2$  (RE = Gd, Y and Yb) are an interesting family of materials that can be used as laser host media for lanthanide doping ( $\text{Ln}^{3+} = \text{Pr}, \text{Nd}, \text{Ho}, \text{Er}, \text{Tm}$  and Yb) (Kaminskii, 1996). Ytterbium-doped potassium rare earth double tungstates (KREWs) provide broad bandwidths which can make some degree of tunability possible. They can also be efficiently and directly pumped with a diode laser at 940 or 980 nm. All this makes it possible to generate simplified femtosecond lasers and high-power amplifiers based on ytterbium KREW crystals (Brenier, 2001; Boulon, 2003; Krueger & Féru, 2004). These materials are also SRS (simulated Raman scattering) active hosts, so the number of possible laser emissions increases (Grabtchikov, 2000; Narkhova & Ustimenko, 1998; Ustimenko & Gulín, 1998, 2002).  $\text{KLu}(\text{WO}_4)_2$  is isostructural with these materials and is expected to have similar promising optical/physical properties, characterized by a high anisotropy.

The KLuW structure has been studied in the past. Klevtsov & Kozeva (1969) measured the unit-cell parameters of KLuW with X-ray powder patterns: the parameters were  $a = 7.99$ ,  $b = 10.21$ ,  $c = 7.49$  Å. However, they did not mention the space group. Later, the same authors published the unit-cell para-

eters of one of the high-temperature phases of this compound, a trigonal phase, with  $a = 5.91$ ,  $b = 8.04$ ,  $c = 7.31$  Å (Klevtsov *et al.*, 1974). In another paper, Klevtsov *et al.* (1975) again used X-ray diffraction powder patterns to obtain the unit-cell parameters of the monoclinic phase:  $a = 10.51$ ,  $b = 10.21$ ,  $c = 7.45$  Å,  $\beta = 130.5^\circ$ , in space group  $C2/c$ . Later, Yudanov *et al.* (1986) used X-ray diffraction patterns to determine the unit-cell parameters  $a = 10.592$  (3),  $b = 10.236$  (6),  $c = 7.498$  (1) Å,  $\beta = 130.75$  (2)°, in the space group  $I2/c$ . As we have reported in a previous article (Pujol, Solé *et al.*, 2001), and in agreement with Kaminskii *et al.* (2002), unit-cell parameters of KREW can be expressed in three equivalent correct crystallographic settings:  $C2/c$ ,  $I2/c$  and  $I2/a$ , with the appropriate cell dimensions in each case. Kaminskii *et al.* (1998) reported the crystallographic data as  $a = 7.99$ ,  $b = 10.21$ ,  $c = 7.45$  Å,  $\beta = 94^\circ$ , expressed in  $I2/c$  for KLuW material. According to the recommendations of the International Union of Crystallography regarding the standard setting, we have redetermined the structure of KLuW and expressed it in the  $C2/c$  crystallographic setting. In the present paper, unit-cell parameters and fractional atomic coordinates are presented and interatomic distances are described in detail. Because of the monoclinic structure of this material, its physical properties are thought to be considerably anisotropic. Further applications of this material as a host laser single

crystal make it necessary to determine this anisotropy in the thermal and mechanical properties in detail, such as the linear thermal expansion and microhardness.

The Yb<sup>3+</sup> ion is recognized as a potentially interesting dopant for InGaAs diode-pumped solid-state lasers in the 1 μm region (DeLoach *et al.*, 1993; Zou & Toratani, 1995; Krupke, 2000). The similar ionic radii (coordination number 8) of Yb<sup>3+</sup> (0.985 Å) and Lu<sup>3+</sup> (0.977 Å) ions and, consequently, the foreseen similarity between the cell parameters of KLuW and KYbW, make it possible to obtain highly Yb-doped KLuW layers on KLuW substrates with high quality (Griebner, Liu *et al.*, 2005). Highly doped materials with active ions are potentially interesting for thin-disc laser design; these materials have demonstrated their potential for high-output powers (Stewen *et al.*, 2005). KLuW can also incorporate high doping ytterbium concentrations with no important changes in the structure, as is reported in the present paper. Continuous wave (CW) highly efficient and mode-locked laser emission has been achieved very recently in ytterbium KLuW material both in bulk and epitaxial configuration (Mateos *et al.*, 2004; Griebner, Rivier *et al.*, 2005; Rivier *et al.*, 2005).

We present our structural studies of KLuW as a competitive host for ytterbium laser ions. The change in the unit-cell parameters due to the partial substitution of Lu by Yb is also reported. These results complement the laser performance in the system Yb:KLuW.

## 2. Structure of KLu(WO<sub>4</sub>)<sub>2</sub>

The single crystals used for the structural studies were obtained from high-temperature solutions, with K<sub>2</sub>W<sub>2</sub>O<sub>7</sub> as a solvent, and a solution composition of 12 mol% solute and 88 mol% solvent. The crystals nucleated on a platinum disc, 12 mm in diameter, rotating at 40 r.p.m. in the homogeneous solution. The crystals grew because of the supersaturation created by decreasing the temperature to about 10 K from the saturation temperature with a cooling rate of around 0.5–1 K h<sup>-1</sup>.

Single-crystal X-ray diffraction data of KLuW were collected and then the structure was solved by Patterson synthesis using the *SHELXS97* computer program (Sheldrick, 1997), followed by refinement by the full-matrix least-squares method using *SHELXL97* (Sheldrick, 1997). The space group was *C2/c* of the monoclinic system and the unit-cell parameters were *a* = 10.576 (7), *b* = 10.214 (7), *c* = 7.487 (2) Å, β = 130.68 (4)°. Table 1 shows this information as well as the crystal data, data collection and refinement details. The atomic positions and interatomic distances are summarized in Tables 2 and 3, respectively.<sup>1</sup>

The structure is close to that of other KREW structures (Pujol, Solé *et al.*, 2001; Pujol *et al.*, 2002; Klevtsov *et al.*, 1968; Borowiec *et al.*, 2003; Kaminskii *et al.*, 1998). As in the other potassium double tungstates, the coordination figure of the

**Table 1**

Crystal data, data collection and refinement parameters of monoclinic KLu(WO<sub>4</sub>)<sub>2</sub>.

Crystal data	Mo Kα radiation
KLu(WO <sub>4</sub> ) <sub>2</sub>	λ = 0.71069 Å
<i>M<sub>r</sub></i> = 709.77	Cell parameters from 25 reflections
Monoclinic, <i>C2/c</i>	θ = 12–21°
<i>a</i> = 10.576 (7) Å	μ = 54.071 mm <sup>-1</sup>
<i>b</i> = 10.214 (7) Å	<i>T</i> = 293 (2) K
<i>c</i> = 7.487 (2) Å	Sphere
β = 130.68 (4)°	0.2 mm diameter
<i>V</i> = 613.3 (6) Å <sup>3</sup>	Colourless
<i>Z</i> = 4	
<i>D<sub>x</sub></i> = 7.686 Mg m <sup>-3</sup>	
Data collection	
Enraf–Nonius CAD-4 diffractometer	<i>R</i> <sub>int</sub> = 0.0343
ω–2θ scans	θ <sub>max</sub> = 29.97°
Absorption correction: spherical	<i>h</i> = –14→11
1875 measured reflections	<i>k</i> = 0→14
899 independent reflections	<i>l</i> = 0→10
664 reflections with <i>I</i> > 2σ( <i>I</i> )	3 standard reflections every 120 min
	Intensity decay: none
Refinement	
Refinement on <i>F</i> <sup>2</sup>	(Δ/σ) <sub>max</sub> = 0.002
<i>R</i> [ <i>F</i> <sup>2</sup> > 2σ( <i>F</i> <sup>2</sup> )] = 0.0356	Δρ <sub>max</sub> = 0.766 e Å <sup>-3</sup>
<i>wR</i> ( <i>F</i> <sup>2</sup> ) = 0.0824	Δρ <sub>min</sub> = –0.673 e Å <sup>-3</sup>
<i>S</i> = 1.209	Extinction correction: none
899 reflections	Scattering factors from <i>International Tables for Crystallography</i> (Vol. C)
56 parameters	
<i>w</i> = 1/[σ <sup>2</sup> ( <i>F</i> <sub>o</sub> <sup>2</sup> ) + (0.0275 <i>P</i> ) <sup>2</sup> ]	
where <i>P</i> = ( <i>F</i> <sub>o</sub> <sup>2</sup> + 2 – <i>F</i> <sub>c</sub> <sup>2</sup> )/3	

**Table 2**

Fractional atomic coordinates and equivalent isotropic displacement parameters (Å<sup>2</sup>) of KLu(WO<sub>4</sub>)<sub>2</sub>.

	Wyckoff position	<i>x</i>	<i>y</i>	<i>z</i>	<i>U</i> <sub>eq</sub>
Lu	4 <i>e</i>	0	0.72841 (3)	1/4	0.01989 (19)
W	8 <i>f</i>	0.19691 (3)	0.00005 (2)	0.73532 (5)	0.01801 (16)
K	4 <i>e</i>	1/2	0.2027 (3)	3/4	0.0249 (6)
O1	8 <i>f</i>	0.3768 (7)	–0.0828 (7)	0.8121 (13)	0.0462 (16)
O2	8 <i>f</i>	0.0239 (7)	–0.1070 (6)	0.4722 (11)	0.0334 (12)
O3	8 <i>f</i>	0.2835 (7)	0.1522 (6)	0.8784 (13)	0.0418 (16)
O4	8 <i>f</i>	0.2003 (6)	–0.0749 (8)	0.9536 (12)	0.0402 (14)

tungstate anion is a distorted octahedron, WO<sub>6</sub> [W–O distances range from 1.767 (7) to 2.265 (8) Å]. The units, which are formed by two distorted octahedra that share the edges O2–O2<sup>i</sup> [2.341 (9) Å; symmetry code: (i) –*x*, –*y*, 1 – *z*], make up the characteristic double chain in the crystallographic *c* direction by sharing vertex O4. Observing the distances W–O along the series KREW (RE = Gd, Yb and Lu), in KLuW there is an increase of the regularity of the coordination figure. We calculated the degree of distortion, Δ<sub>*d*</sub>, of the coordination polyhedra with

$$\Delta_d = (1/n) \sum_{i=1}^n \left\{ \frac{[d(M-O)_n - \langle d(M-O) \rangle]}{\langle d(M-O) \rangle} \right\}^2$$

(Carvajal *et al.*, 2003). The results are summarized in Table 4. The average W–O distance decreases along KREW (RE = Gd, Yb and Lu) so we can expect the WO<sub>6</sub> groups in the KLuW host to be more compact and more covalent.

<sup>1</sup> Full crystallographic data (CIF and structure factors) are available from the IUCr electronic archives (Reference: K55080). Services for accessing these data are described at the back of the journal.

**Table 3**  
Selected interatomic distances (Å) of monoclinic KLu(WO<sub>4</sub>)<sub>2</sub>.

W—O3	1.767 (7)	Lu—O2 <sup>iii</sup>	2.260 (7)	K—O4 <sup>vii</sup>	2.786 (8)	W—W <sup>i</sup>	3.261 (2)
W—O4	1.784 (8)	Lu—O1 <sup>iv</sup>	2.217 (9)	K—O4 <sup>ii</sup>	2.739 (6)	W—W <sup>ii</sup>	3.743 (3)
W—O1	1.801 (6)	Lu—O3 <sup>v</sup>	2.299 (7)	K—O1 <sup>ii</sup>	2.894 (8)	W—W <sup>ix</sup>	3.744 (3)
W—O2	1.930 (6)	Lu—O3 <sup>vi</sup>	2.765 (6)	K—O2 <sup>viii</sup>	2.976 (7)	W—Lu <sup>x</sup>	3.513 (2)
W—O2 <sup>i</sup>	2.081 (6)			K—O3	3.050 (8)	W—Lu <sup>xi</sup>	3.803 (3)
W—O4 <sup>ii</sup>	2.265 (8)			K—O1	3.348 (7)	W—Lu <sup>xii</sup>	3.908 (3)
						W—Lu <sup>xiii</sup>	3.921 (3)
						W—K <sup>ix</sup>	3.648 (3)
						W—K <sup>xiv</sup>	3.803 (3)
						W—K	3.757 (3)
						Lu—K <sup>v</sup>	3.753 (3)
						Lu—K <sup>xv</sup>	3.753 (3)
						Lu—Lu <sup>xvi</sup>	4.045 (3)
						Lu—Lu <sup>vi</sup>	5.982 (3)
						Lu—Lu <sup>xvii</sup>	6.693 (3)

Symmetry codes: (i)  $-x, -y, 1 - z$ ; (ii)  $x, -y, z - \frac{1}{2}$ ; (iii)  $x, 1 + y, z$ ; (iv)  $\frac{1}{2} - x, \frac{1}{2} - y, 1 - z$ ; (v)  $x - \frac{1}{2}, \frac{1}{2} + y, z - 1$ ; (vi)  $x, 1 - y, z - \frac{1}{2}$ ; (vii)  $\frac{1}{2} + x, \frac{1}{2} + y, z$ ; (viii)  $\frac{1}{2} - x, \frac{1}{2} + y, \frac{3}{2} - z$ ; (ix)  $x, -y, \frac{1}{2} + z$ ; (x)  $x, 1 - y, \frac{1}{2} + z$ ; (xi)  $\frac{1}{2} + x, y - \frac{1}{2}, 1 + z$ ; (xii)  $\frac{1}{2} + x, \frac{1}{2} - y, \frac{1}{2} + z$ ; (xiii)  $x, y - 1, z$ ; (xiv)  $x - \frac{1}{2}, y - \frac{1}{2}, z$ ; (xv)  $x - \frac{1}{2}, \frac{1}{2} + y, z$ ; (xvi)  $\frac{1}{2} - x, \frac{3}{2} - y, 1 - z$ ; (xvii)  $x, 2 - y, z - \frac{1}{2}$ .

**Table 4**  
Structural and optical parameters for KREW (RE = Gd, Yb and Lu).

	KGdW	KYbW	KLuW
IR (RE) (Å)	1.053	0.985	0.977
<i>a</i> (Å)	10.652 (4)	10.590 (4)	10.576 (7)
<i>b</i> (Å)	10.374 (6)	10.290 (6)	10.214 (7)
<i>c</i> (Å)	7.582 (2)	7.478 (2)	7.487 (2)
$\beta$ (°)	130.80 (2)	130.70 (2)	130.68 (4)
<i>V</i> (Å <sup>3</sup> )	634.2 (5)	617.8 (5)	613.3 (6)
$\Delta_{W-O}$ ( <i>n</i> = 6)	12.4 (7)	10.7 (4)	8.8 (4)
$\Delta_{RE-O}$ ( <i>n</i> = 8)	1.8 (5)	3.8 (4)	4.3 (5)
$\Delta_{K-O}$ ( <i>n</i> = 12)	1.8 (1)	3.0 (1)	2.3 (1)
<i>H<sub>v</sub></i> (100)	—	—	440
<i>H<sub>v</sub></i> (010)	—	—	410
<i>H<sub>v</sub></i> (001)	—	—	560
Hardness (Moh's scale)	4.5–5	—	4–5.5
$\alpha'_{11}$	10.64	8.72	8.98
$\alpha'_{22}$	2.83	2.57	3.35
$\alpha'_{33}$	23.44	16.68	16.72
$\alpha'_{33}/\alpha'_{11}$	2.21	1.91	1.86
$\kappa$	21.5 (5)	19 (5)	18.5 (5)
$2V_g$ ( $\lambda$ = 1064 nm, RT)	94.57	88.14	82.03
$\sigma_{OA}$ (cm <sup>2</sup> ) for <i>E</i>    <i>N<sub>m</sub></i> at 981.1 nm	$1.2 \times 10^{-19}\dagger$	$1.17 \times 10^{-19}\ddagger$	$1.18 \times 10^{-19}$
$\sigma_{OE}$ (cm <sup>2</sup> ) for <i>E</i>    <i>N<sub>m</sub></i> at 981.1 nm	$1.46 \times 10^{-19}\dagger$	$1.47 \times 10^{-19}$	$1.47 \times 10^{-19}$

† Brenier & Boulon (2001), Bourdet (2001). ‡ Pujol, Bursukova *et al.* (2001).

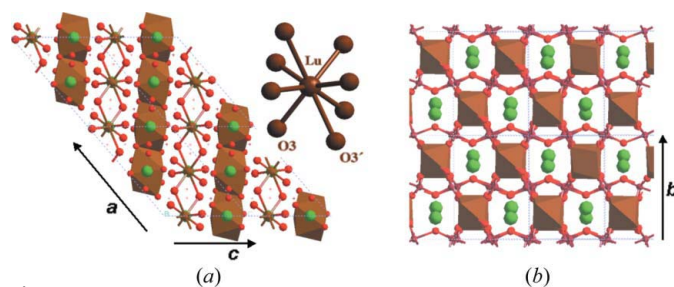


**Figure 1**  
Projections of the crystalline structure of KLu(WO<sub>4</sub>)<sub>2</sub>. (a) Parallel to the *b* direction; the chain formed by lutetium polyhedra is along the [101] direction. Inset: the coordination figure of the lutetium ion. (b) Parallel to the [101] direction; the lutetium zigzag chain polyhedra are perpendicular to the observer.

The lutetium is eightfold coordinated by oxygen atoms to form a distorted square antiprism. These polyhedra form a single chain in the [101] direction by sharing the O3—O3<sup>xviii</sup> edges [3.081 (11) Å; symmetry code: (xviii)  $\frac{1}{2} - x, \frac{1}{2} - y, 2 - z$ ]. This shared edge, O3—O3<sup>xviii</sup> [3.081 (11) Å], increases in length along the KREW series RE = Gd, Yb and Lu (Pujol, Solé *et al.*, 2001; Pujol *et al.*, 2002) (see Fig. 1a). This is because the positive charge in the nucleus of the lanthanide element increases, so there is a corresponding increase in the strength of one of the Lu—O bonds, Lu—O3<sup>v</sup> [2.299 (7) Å; symmetry code: (v)  $x - \frac{1}{2}, \frac{1}{2} + y, z - 1$ ], which means that one oxygen from this edge is getting closer to a lutetium

anion. As a consequence of this elongation in the shared edge O3—O3<sup>xviii</sup>, the distortion of the coordination figure in the KREW increases. Table 4 summarizes these values.

The values of the Lu—Lu distances should also be mentioned, because of their importance in further substitutions by active lanthanide ions and energy-transfer phenomena between lanthanide ions (Kushida, 1973; Inokuti & Hirayama, 1965; Huber *et al.*, 1977). Each LuO<sub>8</sub> chain is parallel to the [101] direction and forms a zigzag, where the Lu—Lu<sup>xvi</sup> distances within a chain are 4.045 (3) Å [symmetry code: (xvi)  $\frac{1}{2} - x, \frac{3}{2} - y, 1 - z$ ]. Furthermore, each lutetium polyhedra chain is surrounded by four other equivalent chains (Fig. 1b) at Lu—Lu<sup>vi</sup> distances of 5.982 (3) Å [symmetry code: (vi)  $x, 1 - y, z - \frac{1}{2}$ ] and Lu—Lu<sup>xvii</sup> distances of 6.693 (3) Å [symmetry code: (xvii)  $x, 2 - y, z - \frac{1}{2}$ ].

This environment is similar to the other KREW compounds, with corresponding distances of 4.070 (2), 6.057 (2) and 6.804 (2) Å in KGdW, and 4.049 (2), 6.009 (2) and 6.721 (2) Å in KYbW.

### 2.1. Effects of doping: unit-cell parameter changes with ytterbium doping

The change in the unit-cell parameters can be measured to predict the structural changes related to doping. The unit-cell parameters of Yb:KLuW were obtained by X-ray powder diffraction analysis, using a Siemens D-5000 diffractometer (Bragg–Brentano parafocusing geometry and vertical  $\theta$ – $\theta$  goniometer). The X-ray powder diffraction patterns were recorded at  $2\theta = 10$ – $70^\circ$ , step size =  $0.02^\circ$ , step time = 16 s. The samples were obtained with [Yb<sup>3+</sup>] concentrations of 10, 20 and 50 (% solute in moles). The real composition in the crystal was calculated taking into account the distribution coefficient of ytterbium in KLuW from our growth experiences, which was obtained by electron microprobe analysis, as we shall describe below. As expected, the structure remains monoclinic in all cases [the isostructural material KYbW with 100 mol% ytterbium is also monoclinic (Pujol *et al.*, 2002)]. In order to obtain the cell parameters, the X-ray patterns were fitted using

the *FullProf* program (Rodriguez-Carvajal, 2000) and the structural model obtained for KLuW was fitted by single-crystal diffraction. Fig. 2 shows how the unit-cell parameters of KLuW increase with the ytterbium doping. The unit-cell parameters *a*, *b* and *c* increase and  $\beta$  remains basically constant when ytterbium concentrations increase. This increase is expected because the ionic radius of ytterbium (0.985 Å) increases in relation to that of lutetium (0.977 Å) (Shannon, 1976).

### 3. Crystal growth of KLuW and Yb:KLuW

We synthesized undoped KLuW and Yb-doped KLuW bulk single crystals at several dopant concentrations by means of the top-seeded solution growth (TSSG) slow-cooling method as described by Solé *et al.* (1996), with a composition of 12/88 mol% solute/solvent (K<sub>2</sub>W<sub>2</sub>O<sub>7</sub>). The dopant concentration ranged from 0.5 mol% to 25 mol% in solution. The temperature gradient in the solution was 0.1 K mm<sup>-1</sup> and the saturation temperature was between 1146 and 1162 K. The crystals grew by a seed parallel to the **b** crystallographic direction, with no inclusions or macroscopic defects. A cooling interval of 20 K with a cooling rate of 0.1–0.3 K h<sup>-1</sup> was used. Inclusion-free crystals of around 4 g and dimensions of 11 × 7 × 13 mm along the **a**\* × **b** × **c** crystallographic directions were obtained in these conditions.

By way of example, Fig. 3 shows a photograph and a morphological scheme of a KLuW single crystal. The morphology obtained is basically similar to that of the other KREW tungstates, which we obtained with a similar methodology (Solé *et al.*, 1996; Pujol, Solé *et al.*, 2001; Pujol *et al.*, 2002). The present faces are: {110}, { $\bar{1}11$ }, {010} and {310}. It is worth pointing out how important the external appearance of face (010) is in these KREW materials for their laser applications, and also as a structural reference so that samples can be prepared for further optical applications.

It has been observed that when similar growth methodologies are used, the area of face (010) tends to decrease along

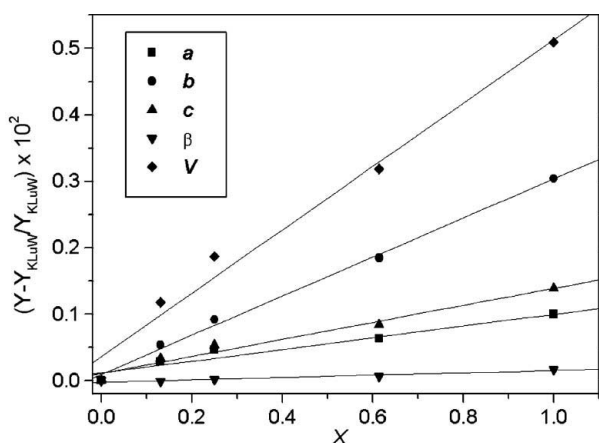


**Figure 2**  
Change in cell parameters (%) of KLuW when the level of substitution of lutetium by ytterbium is increased in the crystal.

**Table 5**  
Summary of the EPMA results of the analysis of Yb<sup>3+</sup>:KLuW.

	$K_{Yb^{3+}}$	[Yb <sup>3+</sup> ] (cm <sup>-3</sup> )	Stoichiometric formula
0.5%	1.39	$4.52 \times 10^{19}$	KLu <sub>0.993</sub> Yb <sub>0.007</sub> (WO <sub>4</sub> ) <sub>2</sub>
3%	1.45	$2.83 \times 10^{20}$	KLu <sub>0.986</sub> Yb <sub>0.043</sub> (WO <sub>4</sub> ) <sub>2</sub>
5%	1.37	$4.30 \times 10^{20}$	KLu <sub>0.931</sub> Yb <sub>0.069</sub> (WO <sub>4</sub> ) <sub>2</sub>
10%	1.30	$8.26 \times 10^{20}$	KLu <sub>0.870</sub> Yb <sub>0.130</sub> (WO <sub>4</sub> ) <sub>2</sub>
25%	1.24	$2.02 \times 10^{21}$	KLu <sub>0.690</sub> Yb <sub>0.310</sub> (WO <sub>4</sub> ) <sub>2</sub>
50%	1.22	$3.99 \times 10^{21}$	KLu <sub>0.390</sub> Yb <sub>0.610</sub> (WO <sub>4</sub> ) <sub>2</sub>

the series KREW (RE = Gd, Yb and Lu). This means that the rate of growth of this face increases along the series.

Electron probe microanalysis (EPMA) was used to determine the concentration of Yb<sup>3+</sup> in the crystals. The line  $M\alpha$ , the detector crystal TAP and a homemade KYbW standard were used to minimize the error caused by the different compositions of the sample and standard. The distribution coefficient of the doping element,  $K_{Yb^{3+}}$ , was calculated by

$$K_{Yb^{3+}} = \frac{[\text{moles Yb}^{3+} / (\text{moles Yb}^{3+} + \text{moles Lu}^{3+})]_{\text{crystal}}}{[\text{moles Yb}^{3+} / (\text{moles Yb}^{3+} + \text{moles Lu}^{3+})]_{\text{solution}}}$$

for the composition 12 mol% Yb:KLuW/88 mol% K<sub>2</sub>W<sub>2</sub>O<sub>7</sub>. The results, presented in Table 5, show a very high distribution coefficient of Yb<sup>3+</sup> inside the host, which suggests the feasibility of doping this compound with ytterbium. However, values larger than 1 may create a gradient of ytterbium distribution inside the crystal during the growth process. For further industrial crystal growth of large single crystals of Yb:KLuW, this handicap can be overcome by using an ytterbium feeder in the solution during the crystal growth.

### 4. Microhardness measurements

For solid-state laser (SSL) and optical applications in general, samples must be previously cut and polished if results are to be good. The quality of the polishing of a given sample is directly related to the mechanical properties of the material, and significantly high hardness values can assure a better polish and quality of the laser surfaces.

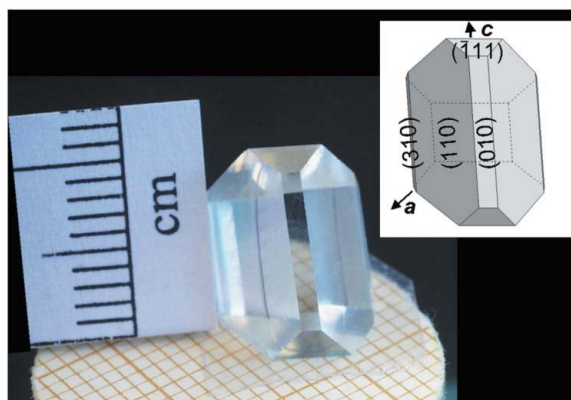


**Figure 3**  
Monoclinic KLuW crystal grown in the **b** direction. Inset: morphological scheme.

Vickers microhardness measurements were made on three different faces of the KLuW single crystals. The measured faces were cut perpendicular to the three crystallographic directions **a\***, **b** and **c**, respectively. The indenter used was a Vickers diamond square-based pyramid (Vander Voort, 1989). The strengths used were 0.03 N, 0.05 N and 0.1 N. For each load, different indentations were made and the average diagonal imprints were used for the calculation. Scanning electron microscope (Jeol JSM 6400 equipment) images were used to quantify the diagonal imprint of the residual indentation impression.

The measured microhardness values,  $H_V$ , were 440, 410 and 560 (see Table 4) on the planes perpendicular to **a\***, **b** and **c**, respectively. It is important to point out the expected anisotropy in the different crystallographic directions of our materials. Furthermore, the Vickers value ( $H_V$ ) of the (010) face is 410, which is around 4 on Moh's scale. This means that the polishing procedure on face (010) would not be any better than on any other faces of our crystal.

### 5. Thermal expansion tensor

The pumping process in the laser cavity generates heat in the laser system. In spite of the cooling or refrigeration system, there will be energy losses, which transform into heat. The thermal stability of the geometry of the sample in the laser device can be improved or predicted, if the anisotropic linear thermal expansion of the laser material KREW is known. KREW materials also present anisotropy in thermal properties. A good laser cavity design must take into account this anisotropy at temperatures higher than room temperature. For these reasons, and also because linear thermal expansion is related to the thermo-optical coefficients (Biswal *et al.*, 2004), which need to be known for laser materials, the determination of the linear thermal expansion tensor is important.

As before, the unit-cell parameters of KLuW were measured as a function of temperature by X-ray powder diffraction analysis, and using a Siemens D-5000 diffractometer (Bragg–Brentano parafocusing geometry and vertical  $\theta$ – $\theta$  goniometer) equipped with a high-temperature chamber (Anton-Paar HTK10). The X-ray powder diffraction patterns were recorded at  $2\theta = 10$ – $70^\circ$ , step size =  $0.03^\circ$ , step time = 5 s, at temperatures of 298, 323, 373, 473, 573, 673 and 773 K. The samples were placed on a platinum support. The range of temperatures chosen was large enough for the behaviour of the unit-cell parameters to be described under the conditions to which the crystal is submitted during the pumping process.

In order to obtain the cell parameters, the X-ray patterns were fitted using the *FullProf* program and the structural model was obtained for KLuW by single-crystal diffraction. Table 6 summarizes the evolution of the KLuW unit-cell parameters at different temperatures. The unit-cell para-

**Table 6**  
Evolution of the unit-cell parameters of KLuW at different temperatures.

Temperature (K)	<i>a</i> (Å)	<i>b</i> (Å)	<i>c</i> (Å)	$\beta$ (°)	<i>V</i> (Å <sup>3</sup> )
298	10.5898 (5)	10.2362(5)	7.4962 (3)	130.7445 (2)	615.64 (5)
323	10.5945 (4)	10.2375 (3)	7.5004 (2)	130.7487 (2)	616.29 (4)
373	10.6000 (4)	10.2406 (4)	7.5059 (3)	130.7508 (2)	617.23 (5)
473	10.6114 (4)	10.2425 (4)	7.5176 (3)	130.7587 (3)	618.91 (4)
573	10.6214 (5)	10.2470 (5)	7.5298 (3)	130.7624 (3)	620.73 (5)
673	10.6332 (5)	10.2502 (4)	7.5424 (3)	130.7760 (3)	622.52 (5)
773	10.6441 (6)	10.2525 (5)	7.5556 (4)	130.7835 (4)	624.32 (6)

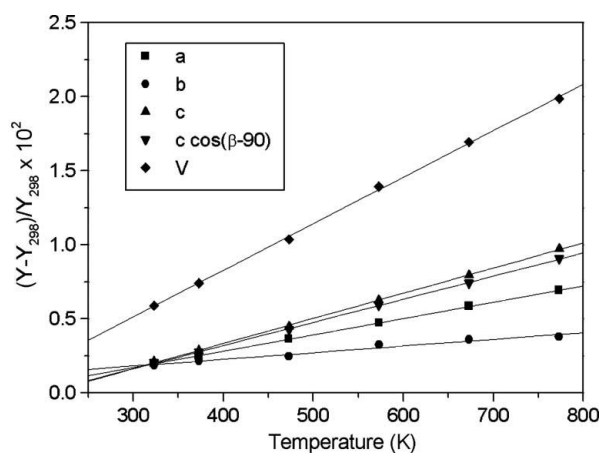


**Figure 4**  
Relative thermal evolution of the cell parameters and the unit-cell volume for monoclinic KLuW.

eters *a*, *b* and *c* increase and  $\beta$  remains basically constant when the temperature rises.

The values of the linear thermal expansion coefficients are the slopes of the linear relationship between  $(\Delta L/L)$  and temperature in the different crystallographic directions (Chung *et al.*, 1993). The values for the monoclinic KLuW are  $\alpha_{100} = 10.6 (2) \times 10^{-6}$ ,  $\alpha_{010} = 3.35 (2) \times 10^{-6}$ ,  $\alpha_{001} = 16.3 (2) \times 10^{-6}$ ,  $\alpha_{c^*} = 15.1 (1) \times 10^{-6}$ ,  $\alpha_V = 29.2 (3) \times 10^{-6} \text{ K}^{-1}$ ; see Fig. 4. From these results and the expression  $\alpha_n = n_i n_j \alpha_{ij}$ , where  $n = (n_1, n_2, n_3)$ , we obtain  $\alpha_{13}$ , and, in this way, the linear thermal expansion tensor at 298 K in the crystallophysical system  $X_1||\mathbf{a}$ ,  $X_2||\mathbf{b}$ ,  $X_3||\mathbf{c}^*$  is

$$\alpha_{ij} = \begin{pmatrix} 10.6 & 0 & -3.15 \\ 0 & 3.35 & 0 \\ -3.15 & 0 & 15.1 \end{pmatrix} \times 10^{-6} \text{ K}^{-1}.$$

The linear thermal expansion tensor in the principal system  $X'_1$ ,  $X'_2||\mathbf{b}$ ,  $X'_3$  can be obtained by diagonalizing the above tensor. In monoclinic crystals with  $\beta > 90^\circ$ , the *b* principal axis always coincides with the 2 symmetry axis. In the present study, this axis corresponds to the minimum thermal expansion coefficient,  $X'_2$ . Therefore, the diagonalized linear thermal expansion tensor has the following values:

$$\alpha'_{ij} = \begin{pmatrix} 8.98 & 0 & 0 \\ 0 & 3.35 & 0 \\ 0 & 0 & 16.72 \end{pmatrix} \times 10^{-6} \text{ K}^{-1}.$$

The principal axis with medium thermal expansion,  $X'_1$ , was found at  $\rho = 27.24^\circ$  rotating clockwise from the  $a$  axis with the  $b$  positive axis pointing towards us. Finally, the principal axis with the maximum thermal expansion coefficient,  $X'_3$ , was found at  $\delta = 13.51^\circ$ , with  $\delta = (\beta - 90^\circ) - \rho$  rotating anti-clockwise from the  $c$  axis. The thermal expansion ellipsoid with the values of these angles can be seen in Fig. 5.

The angle between  $X'_3$  and  $c$  of KLuW is similar to that of KREW tungstates (RE = Gd, Y, Er and Yb) (Pujol, Solé *et al.*, 2001). On the other hand, if we observe the linear thermal expansion anisotropy on face (010) (using the ratio  $\alpha'_{33}/\alpha'_{11}$  to determine this anisotropy), we observe that it decreases along the KREW series. Thus, KLuW is the host in the KREW series that has the lowest thermal anisotropy in the (010) plane. This means that it has the least probability of cracking for thermal reasons during the lasing process.

### 6. Refractive index tensor

The monoclinic phase of KLuW belongs to the  $2/m$  crystallographic point group and is therefore a biaxial crystal with inversion centre. The  $N_p$  orthogonal principal crystallo-optic axis is parallel to the  $2(C_2)$  symmetry axes. The other two principal axes are in the  $ac$  plane. The orientation of the

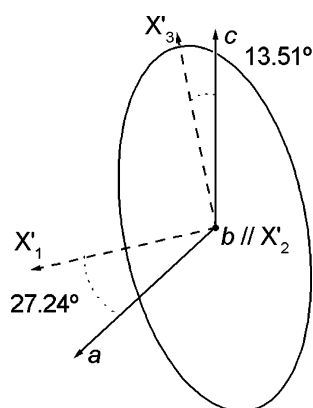


Figure 5 Thermal expansion ellipsoid of KLuW.

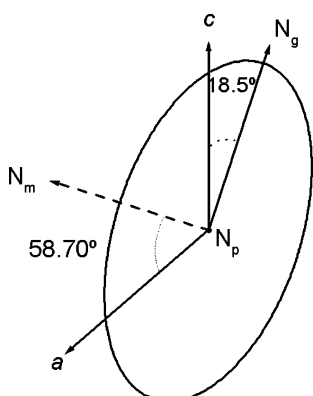


Figure 6 Optical ellipsoid of KLuW at room temperature.

Table 7 Room-temperature Sellmeier coefficients of KLuW.

Principal refractive index	A	B	C (μm)	D (μm <sup>-2</sup> )
$n_g$	3.58334	0.73512	0.26700	0.02953
$n_m$	3.36989	0.74309	0.26193	0.04331
$n_p$	3.21749	0.75382	0.25066	0.05076

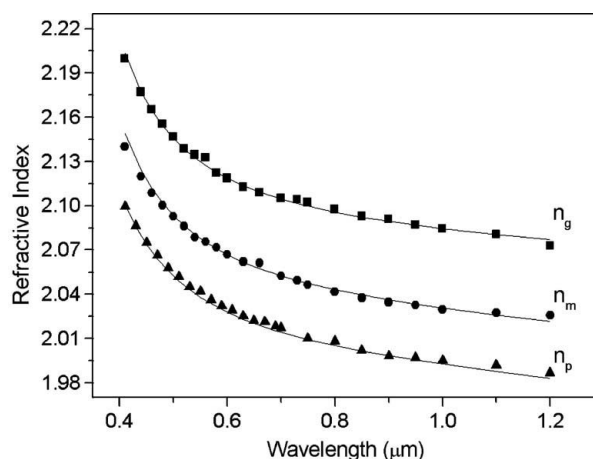


Figure 7 Dispersion of the principal refractive indices of KLuW at room temperature.

principal axes  $N_m$ ,  $N_g$  to the  $c$  axis was determined at  $\lambda = 632.8$  nm by using two crossed Glan–Taylor polarizers. The principal axis  $N_g$  is located at  $\kappa = 18.5^\circ$  clockwise to the  $c$  crystallographic axis when the positive  $b$  axis is pointing towards the observer.  $N_m$  is rotated at  $59.7^\circ$  with respect to the  $a$  crystallographic axis in the clockwise direction. Fig. 6 shows the optical ellipsoid of KLuW. We used the minimum-deviation method with a semiprism (see Solé *et al.*, 2001) to determine the dispersion of the three refractive indices labelled  $n_g$ ,  $n_m$  and  $n_p$  in relation to the wavelength in the range 410–1200 nm at room temperature. Two prisms cut in different principal planes were used. One of the prisms provided  $n_p$  and  $n_m$ , and the other  $n_p$  and  $n_g$  with an accuracy of  $5 \times 10^{-4}$ . Fig. 7 shows the experimental values of refractive indices and the fitted curve using the Sellmeier equation

$$n^2 = A + \frac{B}{1 - (C/\lambda)^2} - D\lambda^2.$$

Table 7 summarizes the Sellmeier coefficients, which characterize KLuW in the visible and near-IR spectral regions. Using these measurements, it is possible to localize the two optic axes. The optic axes are located in the  $N_p N_g$  plane, at an angle of  $V_g$  to the  $N_g$  axis:

$$\sin V_g = \frac{n_g}{n_m} \left( \frac{n_m^2 - n_p^2}{n_g^2 - n_p^2} \right)^{1/2}.$$

For KLuW, at 1064 nm, the  $V_g$  angle is  $41.016^\circ$ , which means that the angle between the two optic axes is  $82.03^\circ$ . Therefore, KLuW is an optically positive biaxial crystal ( $V_g < 45^\circ$ ).

This work was supported by EU project DT-CRYS, NMP3-CT-2003-505580, by CICYT (Comisión Interministerial de Ciencia y Tecnología of the Spanish Government) under the MAT-2002-04603-C05-03 and MAT-2005-06354-C03-02 projects, and by the Generalitat de Catalunya under the projects 2001SGR317 and 2005SGR658.

### References

- Biswal, S. P., O'Connor, S. & Bowman, S. R. (2004). *CLEO/QELS 2004, Conference on Lasers & Electro-Optics CLEO'04*, San Francisco (CA), USA, May 16–21, 2004, paper CThT62, Technical Digest CD-ROM.
- Borowiec, M. T., Majchrowski, A., Domuchowski, V., Dyakonov, V. P., Michalski, E., Zayarniuk, T., Zmija, J. & Szymczak, H. (2003). *Proc. SPIE*, **5136**, 20–25.
- Borowiec, M. T., Watterich, A., Zayarniuk, T., Dyakonov, V. P., Majchrowski, A., Zmija, J., Baranski, M. & Szymczak, H. (2003). *J. Appl. Spectrosc. (Zh. Prikladnoi Spektroskopii, Belarus)*, **70**, 7.
- Boulon, G. (2003). *Opt. Mater.* **22**, 85–87.
- Bourdet, G. L. (2001). *Opt. Commun.* **200**, 331–342.
- Brenier, A. (2001). *J. Lumin.* **92**, 199–204.
- Brenier, A. & Boulon, G. (2001). *J. Alloy. Compd.* **323–324**, 210–213.
- Carvajal, J. J., García-Muñoz, J. L., Solé, R., Gavalda, Jna., Massons, J., Solans, X., Díaz, F. & Aguiló, M. (2003). *Chem. Mater.* **15**, 2338–2345.
- Chung, D. D. L., DeHaven, P. W. & Arnold, H. (1993). *X-ray Diffraction at Elevated Temperatures. A Method for in situ Process Analysis*. New York: Debashis Ghosh VCH.
- Deloach, L. D., Payne, S. A., Chase, L. L., Smith, L. K., Kway, W. L. & Krupke, W. F. (1993). *IEEE J. Quantum Electron.* **29**, 1179–1191.
- Grabtchikov, A. S. (2000). *J. Alloy Compd.* **300–301**, 300–302.
- Griebner, U., Liu, J., Rivier, S., Aznar, A., Grunwald, R., Solé, R., Aguiló, M., Díaz, F. & Petrov, V. (2005). *IEEE J. Quantum Electron.* **41**, 408–414.
- Griebner, U., Rivier, S., Petrov, V., Zom, M., Erbert, G., Weyers, M., Mateos, X., Aguiló, M., Massons, J. & Díaz, F. (2005). *Optics Express*, **13**, 3465–3470.
- Huber, D. L., Hamilton, D. S. & Barnett, B. (1977). *Phys. Rev. B*, **16**, 4642–4650.
- Inokuti, M. & Hirayama, F. (1965). *J. Chem. Phys.* **43**, 1978–1989.
- Kaminskii, A. A. (1996). *Crystalline Lasers: Physical Processes and Operating Schemes*. New York: CRC Press.
- Kaminskii, A. A., Gruber, J. B., Bagaev, S. N., Ueda, K., Hömmerich, U., Seo, J. T., Temple, D., Zandi, B., Kornienko, A. A., Dunina, E. B., Pavlyuk, A. A., Klevtsova, R. F. & Kuznetsov, F. A. (2002). *Phys. Rev. B*, **65**, 125108(1–29).
- Kaminskii, A. A., Ueda, K., Eichler, H. E., Findeisen, J., Bagayev, S. N., Kuznetsov, F., Pavlyuk, A. A., Boulon, G. & Bourgeois, F. (1998). *Jpn J. Appl. Phys.* **37**, L923–L926.
- Klevtsov, P. V. & Kozeva, L. P. (1969). *Sov. Phys.* **14**, 185–187.
- Klevtsov, P. V., Kozeeva, L. P. & Kharchenko, Yu. L. (1975). *Sov. Phys Crystallogr.* **20**, 732–735.
- Klevtsov, P. V., Kozeeva, L. P. & Kletsova, R. F. (1968). *Izv. Akad. SSSR Ser. Neorg. Mater.* **4**, 1147–1151.
- Klevtsov, P. V., Kozeeva, L. P., Kharchenko, Yu. L. & Pavlyuk, A. A. (1974). *Sov. Phys. Crystallogr.* **19**, 342–347.
- Krueger, A. & Féru, P. (2004). *Photonics Spectra*, <http://www.photonics.com>.
- Krupke, W. F. (2000). *IEEE J. Sel. Top. Quantum Electron.* **6**, 1287–1296.
- Kushida, T. (1973). *J. Phys. Soc. Jpn*, **34**, 1318–1325.
- Mateos, X., Petrov, V., Aguiló, M., Solé, R. M., Gavalda, J., Massons, J., Díaz, F. & Griebner, U. (2004). *IEEE J. Quantum Electron.* **40**, 1056–1059.
- Narkhova, G. I. & Ustimenko, N. S. (1998). *Quantum Electron.* **28**, 804–805.
- Pujol, M. C., Bursukova, M. A., Güell, F., Mateos, X., Solé, R., Gavalda, Jna., Aguiló, M., Massons, J., Díaz, F., Klopp, P., Griebner, U. & Petrov, V. (2001). *Phys. Rev. B*, **65**, 165121(1–11).
- Pujol, M. C., Solé, R., Massons, J., Gavalda, Jna., Solans, X., Díaz, F. & Aguiló, M. (2002). *J. Appl. Cryst.* **35**, 108–112.
- Pujol, M. C., Solé, R., Massons, J., Gavalda, Jna., Solans, X., Zaldo, C., Díaz, F. & Aguiló, M. (2001). *J. Appl. Cryst.* **34**, 1–6.
- Rivier, S., Mateos, X., Petrov, V., Griebner, U., Aznar, A., Silvestre, O., Solé, R., Aguiló, M., Díaz, F., Zorn, M. & Weyers, M. (2005). *Opt. Express Lett.* **30**, 2484–2486.
- Rodriguez-Carvajal, J. (2000). *Reference Guide for the Computer Program FullProf*. Laboratoire Léon Brillouin, CEA-CNRS, Saclay, France.
- Shannon, R. D. (1976). *Acta Cryst.* **A32**, 751–767.
- Sheldrick, G. M. (1997). *SHELXS97 and SHELXL97*. University of Göttingen, Germany.
- Solé, R., Nikolov, V., Ruiz, X., Gavalda, Jna., Solans, X., Aguiló, M. & Díaz, F. (1996). *J. Cryst. Growth*, **169**, 600–603.
- Solé, R., Nikolov, V., Vilalta, A., Carvajal, J. J., Massons, J., Gavalda, Jna., Aguiló, M. & Díaz, F. (2001). *J. Mater. Res.* **17**, 563–569.
- Stewen, C., Contag, K., Larinov, M., Giesen, A. & Hügel, H. (2005). *IEEE J. Select Top. Quantum Electron.* **6**, 650–657.
- Ustimenko, N. S. & Gulín, A. V. (1998). *Instrum. Exp. Tech.* **41**, 386–387.
- Ustimenko, N. S. & Gulín, A. V. (2002). *Quantum Electron.* **32**, 229–231.
- Vander Voort, G. F. (1989). *Factors that Affect the Precision of Mechanical Tests*, ASTM STP 1025, pp. 3–39. Philadelphia: ASTM.
- Yudanova, L. I., Potapova, O. G. & Pavlyuk, A. A. (1986). *Izv. Akad. Nauk SSSR Neorg. Mater.* **23**, 1884–1887.
- Zou, X. & Toratani, H. (1995). *Phys. Rev. B*, **52**, 15889–15897.